Two Co(II)-Based MOFs Constructed from Resorcin[4]Arene Ligand: Syntheses, Structures, and Heterogeneous Catalyst for Conversion of CO_2

Bing-Bing Lu [1], Xue Han [2], Cheng-Jie Feng [1], Duo Wang [1],* and Fei Ye [1],*

[1] Department of Chemistry, College of Art and Science, Northeast Agricultural University, Harbin 150030, China; lubingbing@neau.edu.cn (B.-B.L.); fengchengjie@neau.edu.cn (C.-J.F.)

[2] College of Chemistry and Materials Science, Inner Mongolia University for the Nationalities, Tongliao 028000, China; hanx441@nenu.edu.cn

* Correspondence: wang_duo@neau.edu.cn (D.W.); yefei@neau.edu.cn (F.Y.)

Abstract: Two Co(II)-based metal–organic frameworks (MOFs) with open channels, $[(CH_3)_2NH_2]_2$ $[Co_5L(H_2O)_8]\cdot 4H_2O$ (**1**) and $[Co_6L(DMF)_2(H_2O)_8]\cdot 2H_2O$ (**2**), were synthesized using resorcin[4]arene ligand ($H_{12}L$). Compounds **1** and **2** exhibit different 3D microporous framework structures: **1** possesses two kinds of open channels parallel to the a-axis (ca. 5.0×5.0 Å) and the b-axis (ca. 4.0×6.0 Å), and **2** is an open framework with a window size of 5.6×5.6 Å. The activated crystal **1** involves many Lewis acid sites; thus, **1** shows prominent activity and recyclability for the reaction of carbon dioxide coupled with epoxides. Most strikingly, catalyst **1** can be reused for five successive cycles and provides outstanding catalytic activity.

Keywords: MOFs; resorcin[4]arene; Lewis acid; carbon dioxide; epoxides

1. Introduction

Carbon dioxide (CO_2) has caused various environmental and energy problems as a major greenhouse gas, but it is an ideal renewable C1 source in nature [1–4]. Therefore, considerable efforts have been devoted to capturing and converting CO_2 into useful chemical products [5–8], such as CO_2 absorption [9,10], photocatalysis [11–13], electrocatalysis [14–16], and organocatalysis [17–19]. Among these methods, CO_2 coupling with epoxides is regarded as the most effective means because of the 100% atomic availability and the wide use of cyclic carbonates [20–23]. Homogeneous and heterogeneous catalysts have been used to catalyze this reaction, including transition-metal complexes, zeolites, organocatalysts, and so on [24–26]. Although homogeneous catalysts exhibit efficient catalytic activity for the reaction, the inherent limitations of catalyst separation have prevented their wide application [27]. To overcome these drawbacks, heterogeneous catalysts have been considered [28–32]. The cycloaddition reaction between CO_2 and epoxides is a Lewis acid catalysis process; therefore, a catalyst with more active Lewis acid sites provides acceptable conversion of epoxides to cyclic carbonates.

Metal–organic frameworks (MOFs), as a kind of functional material, have attracted tremendous interest due to their large surface area, tunable pore structure, and rich active Lewis acid sites [33–35]. MOFs have a high adsorption capacity for CO_2, which can increase the concentration of CO_2 around the catalytic active sites. Additionally, framework pores can provide confined space for CO_2 reaction [36,37]. Organic linkers play a crucial part in the synthesis of MOFs with a variety of pore size and chemical environments [38–40]. For this application, resorcin[4]arene is especially attractive because of its multiple coordinate sites and tunable structure. Many elegant structures have been obtained using functionalized resorcin[4]arene ligands [41–48].

Herein, we selected a functionalized-resorcin[4]arene ($H_{12}L$) as a ligand, with twelve carboxylate groups in one ligand, so it has multiple possible coordination modes with metal ions.

In this domain, two Co(II)-based microporous structures, $[(CH_3)_2NH_2]_2[Co_5L(H_2O)_8]\cdot4H_2O$ (**1**) and $[Co_6L(DMF)_2(H_2O)_8]\cdot2H_2O$ (**2**), were synthesized using $Co(BF_4)_2\cdot6H_2O$ and $CoCl_2\cdot6H_2O$ with the $H_{12}L$ ligand (Scheme 1). Remarkably, **1** shows outstanding catalytic capability for the conversion of CO_2 as a heterogeneous catalyst.
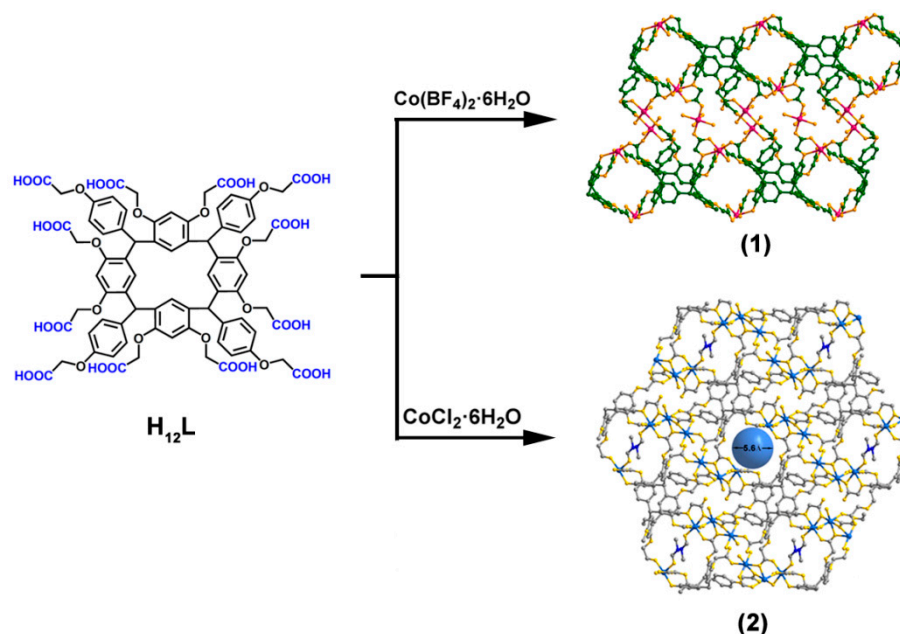
Scheme 1. Synthetic strategy for compounds **1** and **2**.

2. Experimental

2.1. Materials and Methods

All the raw materials were obtained commercially. The method through which the $H_{12}L$ ligand was synthesized is consistent with the literature [49]. The PXRD patterns of **1** and **2** were collected using Cu Kα radiation (λ = 0.154 nm) on a Rigaku Dmax 2000 X-ray diffractometer. ^{1}H NMR spectra were captured on a Bruker 600 MHz spectrometer in CDCl$_3$ or DMSO-d6. TGA data were obtained using a TGA5500 analyzer (5 °C min^{-1}, 25–600 °C, N_2 flow). The C, H, and N elemental analyses were performed using a Vario MACRO cube analyzer. IR spectra were collected on a Thermo Scientific Nicolet 10. The CO_2 gas sorption was performed on V-Sorb 2800S.

2.2. Synthesis of $[(CH_3)_2NH_2]_2[Co_5L(H_2O)_8]\cdot4H_2O$ (**1**)

$H_{12}L$ (0.023 g, 0.015 mmol), $Co(BF_4)_2\cdot6H_2O$ (0.028 g, 0.08 mmol), 4 mL of H_2O, and 4 mL of dimethylformamide (DMF) were mixed in a 15 mL Teflon reactor. The mixture was heated at 100 °C for 72 hours. The pink samples **1** were harvested by filtration (32% yield). Anal. calcd for $C_{80}H_{92}N_2O_{48}Co_5$ (Mr = 2144.20): C, 44.77; H, 4.32; N, 1.31. Found: C, 44.68; H, 4.14; N, 1.29. IR data (KBr, cm^{-1}): 3405 (s), 1606 (s), 1508 (s), 1423 (s), 1322 (m), 1286 (s), 1231 (m), 1184 (m), 1104 (m), 1064 (m), 929 (w), 858 (w), 827(w), 705 (w).

2.3. Synthesis of $[Co_6L(DMF)_2(H_2O)_8]\cdot2H_2O$ (**2**)

$H_{12}L$ (0.015 g, 0.006 mmol) and $CoCl_2\cdot6H_2O$ (0.028 g, 0.12 mmol) were dispersed in DMF/H_2O (8 mL, v/v = 6:2), and then placed in a 15 mL Teflon reactor. The mixture was heated at 110 °C for 72 hours. The pink samples **2** were obtained in a 9% yield. Anal. calcd for $C_{82}H_{86}N_2O_{48}Co_6$ (Mr = 2221.10): C, 44.34; H, 3.90; N, 1.26. Found: C, 43.99; H, 3.86; N, 1.22. IR data (KBr, cm^{-1}): 3415 (s), 1610 (s), 1502 (s), 1421 (s), 1334 (m), 1286 (s), 1162 (m), 1108 (m), 1064 (m), 1064 (m), 930 (w), 858 (w), 825(w), 708 (w).

2.4. Coupling of CO_2 with Epoxides

To obtain the activated sample, catalyst **1** was immersed in acetone for 12 hours and then dried at 60 °C for 10 hours under vacuum. The reactions were executed in a 15 mL flask, the reaction system was refreshed with CO_2 three times, and then the CO_2 pressure was maintained at 1 atm. Epoxide (5 mmol), catalyst **1** (30 mg, 0.0014 mmol), and *n*-Bu$_4$NBr (0.16 g, 0.50 mmol) were mixed in the flask, and then stirred at 80 °C for 8 hours. The conversion of the reactions were calculated by ^{1}H NMR.

2.5. X-ray Crystallography

Diffraction data for compounds **1** and **2** were recorded at room temperature using an Oxford Diffraction Gemini R CCD diffractometer with Mo Kα radiation (λ = 0.71073 Å). The structures of **1** and **2** were solved by direct methods (SHELXS-2014) and refined on F^2 by full-matrix least-squares using the SHELXS-2014 [50–52]. The solvent molecules were highly disordered, so the produced diffused electron densities were removed using the SQUEEZE program in PLATON [53]. Based on the TGA, electron diffraction density, and elemental analysis results, the solvent molecules were directly merged into the final molecular formula. The reflection peaks of hydrogen atoms on the solvent molecules were too weak to assign, so they were directly enclosed in the final molecular formula. Non-H atoms were refined anisotropically. Crystallographic data for **1** (CCDC 2078907) and **2** (CCDC 2078908) are summarized in Table 1, Tables S1 and S2.

Table 1. X-ray crystal data and structure refinements parameters of **1** and **2**.

| Parameters	1	2
Formula	$C_{80} H_{92} O_{48} N_2 Co_5$	$C_{82} H_{86} O_{48} N_2 Co_6$
Mr	2144.20	2221.10
Cryst syst	Triclinic	Triclinic
Space group	*P*-1	*P*-1
a (Å)	10.5320(6)	11.2564(6)
b (Å)	13.2619(7)	15.9785(9)
c (Å)	18.1118(10)	16.5583(10)
α (°)	70.883(5)	62.347(6)
β (°)	74.056(5)	73.527(5)
γ (°)	85.860(4)	70.219(5)
V (Å3)	2297.9(2)	2453.6(3)
Z	1	1
*D*calc (g cm^{-3})	1.550	1.503
F(000)	1105	1138
*R*int	0.0498	0.0446
GOF on F^2	1.211	1.175
R$_1$ [a] [I > 2σ(I)]	0.0847	0.0663
wR$_2$ [b] (all data)	0.1883	0.1559

[a] $R_1 = \Sigma||F_o| - |F_c||/\Sigma|F_o|$. [b] $wR_2 = \{\Sigma[w(F_o^2 - F_c^2)^2]/\Sigma w(F_o^2)^2]\}^{1/2}$.

3. Results and Discussion

3.1. Structure of $[(CH_3)_2NH_2]_2[Co_5L(H_2O)_8]\cdot4H_2O$ (**1**)

Compound **1** crystallizes in the triclinic system with space group *P*-1. Because of the disordered solvents, the SQUEEZE program in PLATON was used during the refinement. There are twelve water molecules and two $[(CH_3)_2NH_2]^+$ cations, produced by the decomposition and protonation of DMF, in the structure [54,55], which was calculated by elemental analysis, TGA, and electron diffraction density. The asymmetric structure of **1** is composed of two and a half CoII cations (Co1, Co2, and Co3), half a L^{12-} ligand, and four coordinated water molecules (Figure 1a). All the Co^{II} cations adopt a six-coordinate mode but different coordination environments. Co1 is coordinated with four water molecules and two O atoms from two L^{12-} ligands; the occupancy of Co1 is 0.5. Co2 is linked with six O atoms from four L^{12-} ligands. Co3 is surrounded by two water molecules and

four O atoms from three L^{12-} ligands. As shown in Figure 1b, each L^{12-} ligand bridges sixteen Co^{II} cations. In this manner, **1** shows a three-dimensional structure. As displayed in Figure 1c,d, there are two types of open channels in the framework with the window sizes of 5.0 × 5.0 Å (Figure 1c) and 4.0 × 6.0 Å (Figure 1d). The solvent-accessible volume is approximately 23.3% (2297.9 Å³), which was estimated by PLATON.
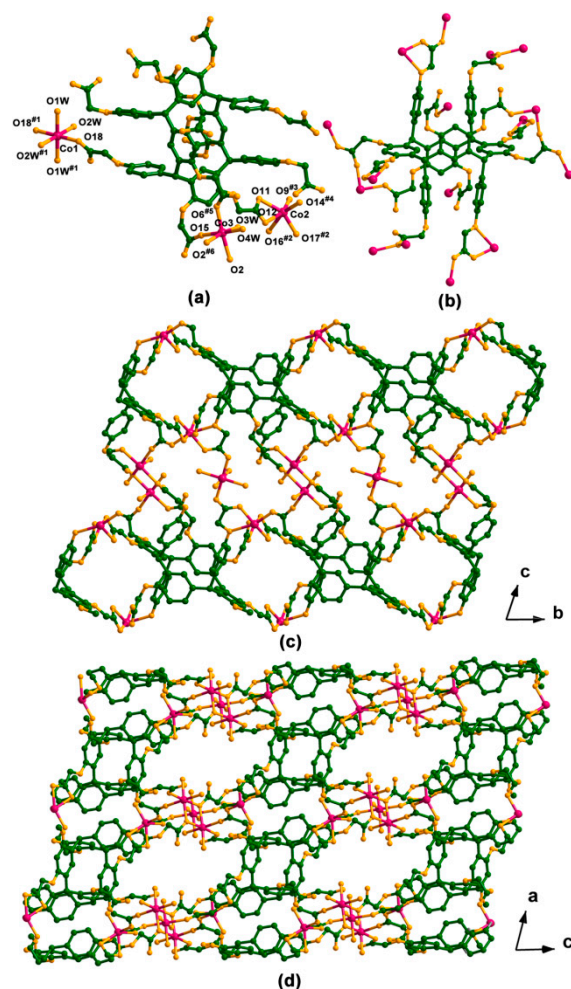
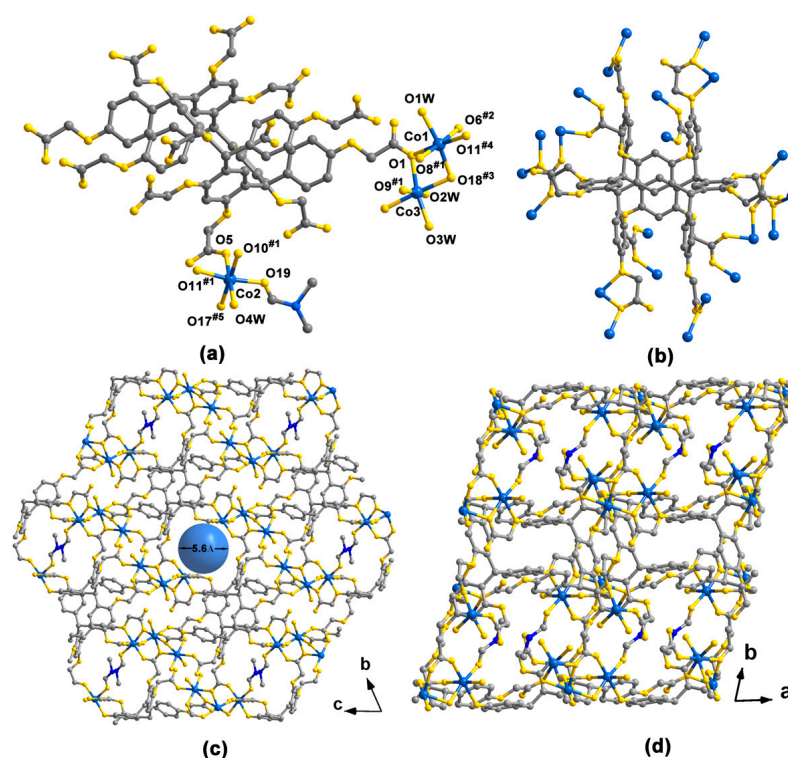

Figure 1. (**a**) Coordination environments around Co(II) in **1**. Symmetry codes: (#1) −x − 2,−y + 2,−z − 1, (#2) −x − 1,−y + 1,−z, (#3) −x,−y + 1,−z, (#4) x + 1,y,z, (#5) x − 1,y,z, and (#6) −x − 1,−y + 2,−z. (**b**) Coordination of the L^{12-} ligand. (**c**) The 1D channel of **1**. (**d**) The 3D framework of **1** down the b-axis.

3.2. Structure of [Co₆L(DMF)₂(H₂O)₈]·2H₂O (2)

The crystal **2** belongs to the triclinic system with space group *P*-1. The SQUEEZE function was used to remove the disordered solvents. The asymmetric structure of **2** comprises three Co^{II} cations (Co1, Co2, and Co3), half a L^{12-} ligand, and four coordinated water molecules (Figure 2a). Compared with Co2 and Co3, Co1 shows different coordination spheres: Co1 is coordinated with one coordinated water molecule and five O atoms from five L^{12-} ligands; Co2 and Co3 both adopt a six-coordinate mode with one coordinated water molecule, one DMF molecule, and four O atoms from three L^{12-} ligands. The Co–O bond lengths vary from 1.993(4) to 2.209(5) Å and the O–Co–O bond angles vary from 58.27(19)° to 180.00(12)°. As illustrated in Figure 2b, every L^{12-} ligand coordinates with twenty-two Co^{II} cations; as such, neighboring L^{12-} ligands are linked by the Co^{II} cations into an open framework. The window size is 5.6 × 5.6 Å along the a axis (Figure 2c,d). The solvent-accessible volume of compound **2** is ca. 20.0% based on the PLATON calculation.

**Figure 2.** (**a**) Coordination environments around Co(II) in **2**. Symmetry codes: (#1) −x + 1,−y + 1,−z − 1, (#2) x − 1,y,z + 1, (#3) x − 1,y − 1,z + 1, (#4) −x,−y + 1,−z, (#5) x,y − 1,z, (#7) x + 1,y,z − 1, (#8) x,y + 1,z, and (#9) x + 1,y + 1,z − 1. (**b**) Coordination of the L^{12-} ligand. The 3D structures of **2** down the a-axis (**c**) and c-axis (**d**).

3.3. Characterization of the Crystal Structure of **1** and **2**

The TGA of compounds **1** and **2** was conducted under a N_2 atmosphere. As displayed in Figure 3a, the TGA of compound **1** indicated that the weight loss before 240 °C is due to the DMF molecules and water molecules, and the framework begins to collapse after 240 °C. The TGA of compound **2** shows that the weight loss before 300 °C belongs to the DMF molecules and water molecules, then the weight loss from 300 °C is attributable to the framework decomposition. The PXRD pattern of **1** is consistent with the simulated one, which indicates that **1** is stable in air. Some characteristic peaks disappeared in the PXRD pattern of **2**, which may have occurred due to an optimum growth orientation being chosen. The CO_2 adsorption was performed at 273 K (Figure S4), and the CO_2 uptake capacity was found to be ca. 0.48 mmol/g.
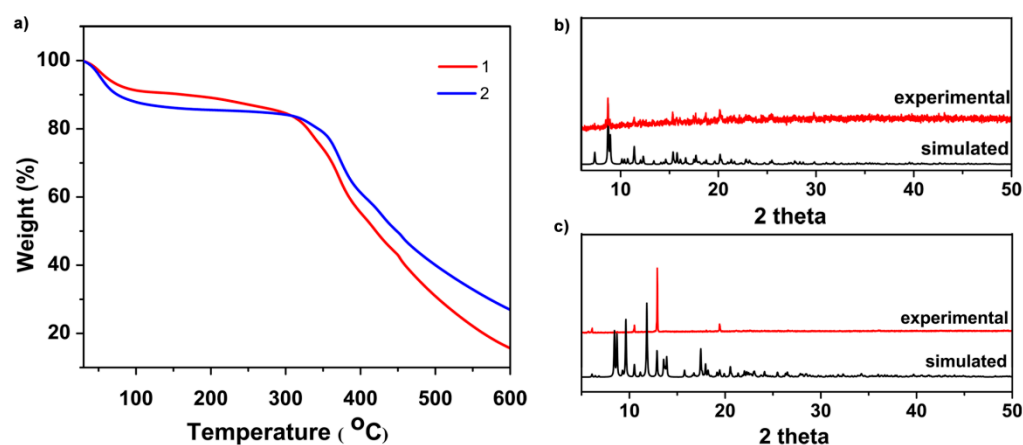
Figure 3. (**a**) Thermogravimetric curves of **1** and **2**. PXRD analysis of (**b**) **1** and (**c**) **2**.

3.4. Coupling of CO_2 with Epoxides

Given the high-density Lewis acid sites and high yield of compound **1**, the heterogeneous catalytic performance of **1** was investigated for the coupling reaction of CO_2 with epoxides. As shown in Scheme 2 and Table 2, gylcidylphenylether was selected as a typical substrate to obtain the optimum reaction conditions. Firstly, the reaction between the gylcidylphenylether and CO_2 was performed in the presence of activated catalyst **1** (10 mg) and *n*-Bu$_4$NBr (0.16 g) at 80 °C for 1 hour; the conversion was only 24% (entry 1, Figure S1a). Thus, the catalyst amount was increased from 10 to 20 and 30 mg, and the corresponding conversions were increased from 24% to 26% and 32%, respectively (entries 2 and 3, Figure S1b,c). The conversion was only 23% when the *n*-Bu$_4$NBr was absent, which indicted that *n*-Bu$_4$NBr is an important co-catalyst (entry 4, Figure S1d). When the reactions were performed at 25 and 50 °C, the conversions were 0% and 12%, respectively (entries 5 and 6, Figure S1e,f). To improve the conversion, the reaction time was extended to 2, 4, 6, and 8 hours; the corresponding conversions were 51%, 80%, 83%, and 98%, respectively (entries 7–10, Figure S1g–j). These experimental results showed that the optimum reaction conditions are 30 mg catalyst **1**, 0.16 g *n*-Bu$_4$NBr, and 1 atm CO_2 reaction at 80 °C for 8 h.
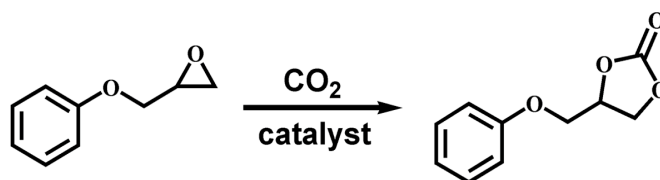
Scheme 2. Coupling of CO_2 with gylcidylphenylether.

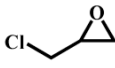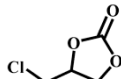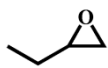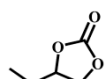**Table 2.** Coupling of CO_2 with gylcidylphenylether under different conditions [a].
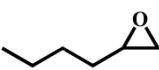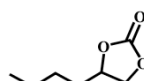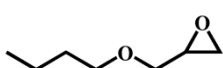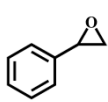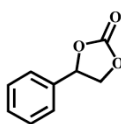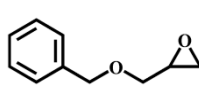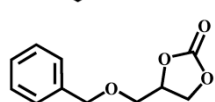
Entry	1 (mg)	Temperature (°C)	Time (h)	Conversion (%) [b]
1	10	80	1	24
2	20	80	1	26
3	30	80	1	48
4	0	80	1	23
5	30	25	1	0
6	30	50	1	12
7	30	80	2	51
8	30	80	4	80
9	30	80	6	83
10	30	80	8	98

[a] Reaction conditions: gylcidylphenylether (5.00 mmol, 0.75 g), *n*-Bu$_4$NBr (0.50 mmol 0.16 g), and CO_2 (1 atm).
[b] Isolated conversions were calculated by ^{1}H NMR.

Different epoxides were selected as the substrates to further examine the applicability of catalyst **1**. The conversions of epichlorohydrin 2-ethyloxirane, 2-butyloxirane, 2-(butoxymethyl)oxirane, 1,2-epoxyethylbenzene and benzylglycidylether were 99%, 99%, 99%, 95%, 75%, and 93%, respectively (entries 1–6 in Table 3, Figure S2a–f). The reaction rate did not decrease when the length of the alkyl chain increased; these experimental results showed that the substrates do not enter the channel but react on the surface of the catalyst (entries 2–4 in Table 3, Figure S2b–d). Compared with other substrates, the reaction of 1,2-epoxyethylbenzene is relatively slow, which may due to the steric-hinderance effect (entries 5 in Table 3, Figure S2e). These results confirmed that the epoxides with variable alkyl chains or aromatic rings are all suitable substrates for the reaction.

Table 3. Coupling of CO_2 with different epoxides [a].

Entry	Epoxides	Products	Conversion (%) [b]
1			99
2			99
3			99
4			95
5			75
6			93

[a] Reaction conditions: epoxides (5.00 mmol), CO_2 pressure (1 atm), activated catalyst **1** (30 mg, 0.07 mmol based on Co^{II} cations), *n*-Bu_4NBr (0.16 g, 0.50 mmol), 8 h, and 80 °C. [b] Isolated conversions were calculated by ^1H NMR.

To further explore the recyclability and stability of **1**, recycling experiments were performed using gylcidylphenylether as the substrate. After the reaction, **1** was recovered from the mixture by centrifugation and filtration and then washed with dichloromethane three times. The catalyst **1** recovered from the reaction was reused for five consecutive cycles with conversions of more than 90% (Figure 4 and Figure S3a–c). This result proved that **1** is a heterogeneous and recyclable catalyst. The PXRD pattern of activated **1** is not consistent with the simulated one, which may due to the single-crystal to single-crystal transition [56]. However, the PXRD pattern of activated **1** after five recycles is consistent with the activated sample, which indicated that **1** is stable during the reaction process (Figure S5).
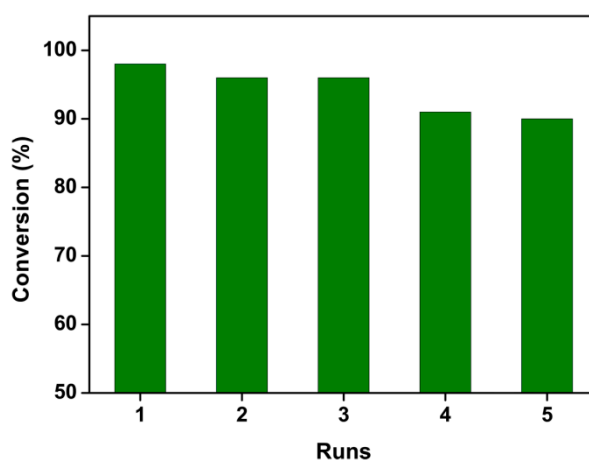
Figure 4. Catalyst recycling test.

4. Conclusions

In summary, we synthesized two microporous MOFs (**1** and **2**) using Co(II) cations and functionalized resorcin[4]arene. The synthesized compounds **1** and **2** were characterized

by single-crystal X-ray diffraction analysis, PXRD, IR, TGA, and elemental analysis. The activated catalyst **1** possesses a large number of unsaturated coordination Co^{II} cations; thus, compound **1** is a promising heterogeneous catalyst for the CO_2 conversion reaction. Most strikingly, **1** can be easily recovered and reused for five consecutive circles with high catalytic activity.

Supplementary Materials: The following are available online at https://www.mdpi.com/article/10.3390/cryst11060574/s1, Figure S1: ^{1}H NMR spectrum of the cycloaddition reaction between CO_2 and gylcidylphenylether; Figure S2: ^{1}H NMR spectrum of CO_2 coupling with different epoxides using **1** as catalysts; Figure S3; ^{1}H NMR spectrum of the cycloaddtion reaction between CO_2 and gylcidylphenylether in different circles; Figure S4. CO_2 total adsorption isotherm for **1**; Figure S5; PXRD patterns of the **1**; Table S1: Selected bond distances (Å) and angles (degrees) for **1**; Table S2: Selected bond distances (Å) and angles (degrees) for **2**. Crystallographic data of **1** and **2** (CIF).

Author Contributions: Conceptualization, B.-B.L., D.W., and F.Y.; data curation, B.-B.L.; formal analysis, B.-B.L. and D.W.; funding acquisition, B.-B.L. and X.H.; investigation B.-B.L.; methodology, B.-B.L.; project administration, B.-B.L.; resources, B.-B.L.; software, B.-B.L. and C.-J.F.; supervision, D.W. and F.Y.; validation, B.-B.L.; visualization, B.-B.L.; writing—original draft, B.-B.L. and X.H.; writing—review and editing, B.-B.L., D.W., and F.Y. All authors have read and agreed to the published version of the manuscript.

Institutional Review Board Statement: Not applicable.

Informed Consent Statement: Not applicable.

Data Availability Statement: Data is contained within the article or supplementary material.

Conflicts of Interest: The authors declare no conflict of interest.

References

1. Artz, J.; Müller, T.E.; Thenert, K.; Kleinekorte, J.; Meys, R.; Sternberg, A.; Bardow, A.; Leitne, W. Sustainable Conversion of Carbon Dioxide: An Integrated Review of Catalysis and Life Cycle Assessment. *Chem. Rev.* **2018**, *118*, 434–504. [CrossRef] [PubMed]
2. He, J.; Janaky, C. Recent Advances in Solar-Driven Carbon Dioxide Conversion: Expectations versus Reality. *ACS Energy Lett.* **2020**, *5*, 1996–2014. [CrossRef] [PubMed]
3. Sumida, K.; Rogow, D.L.; Mason, J.A.; McDonald, T.M.; Bloch, E.D.; Herm, Z.R.; Bae, T.-H.; Long, J.R. Carbon Dioxide Capture in Metal-Organic Frameworks. *Chem. Rev.* **2012**, *112*, 724–781. [CrossRef] [PubMed]
4. Francke, R.; Schille, B.; Roemelt, M. Homogeneously Catalyzed Electroreduction of Carbon Dioxide Methods, Mechanisms, and Catalysts. *Chem. Rev.* **2018**, *118*, 4631–4701. [CrossRef]
5. Yan, X.; Chen, C.; Wu, Y.; Liu, S.; Chen, Y.; Feng, R.; Zhang, J.; Han, B. Efficient electroreduction of CO_2 to C_{2+} products on CeO_2 modified CuO. *Chem. Sci.* **2021**, *12*, 6638–6645. [CrossRef]
6. Jiang, X.; Nie, X.; Guo, X.; Song, C.; Chen, J.G. Recent Advances in Carbon Dioxide Hydrogenation to Methanol via Heterogeneous Catalysis. *Chem. Rev.* **2020**, *120*, 7984–8034. [CrossRef]
7. Ra, E.C.; Kim, K.Y.; Kim, E.H.; Lee, H.; An, K.; Lee, J.S. Recycling Carbon Dioxide through Catalytic Hydrogenation: Recent Key Developments and Perspectives. *ACS Catal.* **2020**, *10*, 11318–11345. [CrossRef]
8. Dey, S.; Bhunia, A.; Breitzke, H.; Groszewicz, P.B.; Buntkowsky, G.; Janiak, C. Two linkers are better than one: Enhancing CO_2 capture and separation with porous covalent triazine-based frameworks from mixed nitrile linkers. *J. Mater. Chem. A* **2017**, *5*, 3609–3620. [CrossRef]
9. Ding, M.; Flaig, R.W.; Jiang, H.-L.; Yaghi, O.M. Carbon capture and conversion using metal-organic frameworks and MOF-based materials. *Chem. Soc. Rev.* **2019**, *48*, 2783–2828. [CrossRef]
10. Yu, J.; Xie, L.-H.; Li, J.-R.; Ma, Y.; Seminario, J.M.; Balbuena, P.B. CO_2 Capture and Separations Using MOFs: Computational and Experimental Studies. *Chem. Rev.* **2017**, *117*, 9674–9754. [CrossRef]
11. Fang, Z.-B.; Liu, T.-T.; Liu, J.; Jin, S.; Wu, X.-P.; Gong, X.-Q.; Wang, K.; Yin, Q.; Liu, T.-F.; Cao, R.; et al. Boosting Interfacial Charge-Transfer Kinetics for Efficient Overall CO_2 Photoreduction via Rational Design of Coordination Spheres on Metal-Organic Frameworks. *J. Am. Chem. Soc.* **2020**, *142*, 12515–12523. [CrossRef] [PubMed]

12. Wang, S.-S.; Huang, H.-H.; Liu, M.; Yao, S.; Guo, S.; Wang, J.-W.; Zhang, Z.-M.; Lu, T.-B. Encapsulation of Single Iron Sites in a Metal-Porphyrin Framework for High-Performance Photocatalytic CO$_2$ Reduction. *Inorg. Chem.* **2020**, *59*, 6301–6307. [CrossRef] [PubMed]

13. Qin, D.; Zhou, Y.; Wang, W.; Zhang, C.; Zeng, G.; Huang, D.; Wang, L.; Wang, H.; Yang, Y.; Lei, L.; et al. Recent advances in two-dimensional nanomaterials for photocatalytic reduction of CO$_2$: Insights into performance, theories and perspective. *J. Mater. Chem. A* **2020**, *8*, 19156–19195. [CrossRef]

14. Zhu, Q.; Yang, D.; Liu, H.; Sun, X.; Chen, C.; Bi, J.; Liu, J.; Wu, H.; Han, B. Hollow metal organic framework-mediated in-situ architecture of copper dendrites for enhanced CO$_2$ electroreduction. *Angew. Chem. Int. Ed.* **2020**, *59*, 8896–8901. [CrossRef] [PubMed]

15. Das, S.; Pérez-Ramírez, J.; Gong, J.; Dewangan, N.; Hidajat, K.; Gates, B.C.; Kawi, S. Core–shell structured catalysts for thermocatalytic, photocatalytic, and electrocatalytic conversion of CO$_2$. *Chem. Soc. Rev.* **2020**, *49*, 2937–3004. [CrossRef] [PubMed]

16. Zhang, L.; Li, X.-X.; Lang, Z.-L.; Liu, Y.; Liu, J.; Yuan, L.; Lu, W.-Y.; Xia, Y.-S.; Dong, L.-Z.; Yuan, D.-Q.; et al. Enhanced Cuprophilic Interactions in Crystalline Catalysts Facilitate the Highly Selective Electroreduction of CO$_2$ to CH$_4$. *J. Am. Chem. Soc.* **2021**, *143*, 3808–3816. [CrossRef]

17. Song, Q.-W.; Zhou, Z.-H.; He, L.-N. Efficient, selective and sustainable catalysis of carbon dioxide. *Green Chem.* **2017**, *19*, 3707–3728. [CrossRef]

18. Shaikh, R.R.; Pornpraprom, S.; D'Elia, V. Catalytic Strategies for the Cycloaddition of Pure, Diluted, and Waste CO$_2$ to Epoxides under Ambient Conditions. *ACS Catal.* **2018**, *8*, 419–450. [CrossRef]

19. Kamphuis, A.J.; Picchioni, F.; Pescarmona, P.P. CO$_2$-fixation into cyclic and polymeric carbonates: Principles and applications. *Green Chem.* **2019**, *21*, 406–448. [CrossRef]

20. Xu, W.; Chen, H.; Jie, K.; Yang, Z.; Li, T.; Dai, S. Entropy-Driven Mechanochemical Synthesis of Polymetallic ZeoliticImidazolate Frameworks for CO$_2$ Fixation. *Angew. Chem. Int. Ed.* **2019**, *58*, 5018–5022. [CrossRef]

21. Ji, H.; Naveen, K.; Lee, W.; Kim, T.S.; Kim, D.; Cho, D.-H. Pyridinium-Functionalized Ionic Metal-Organic Frameworks Designed as Bifunctional Catalysts for CO$_2$ Fixation into Cyclic Carbonates. *ACS Appl. Mater. Interfaces* **2020**, *12*, 24868–24876. [CrossRef] [PubMed]

22. Lu, X.-B.; Darensbourg, D.J. Cobalt Catalysts for The Coupling of CO$_2$ and Epoxides to Provide Polycarbonates and Cyclic Carbonates. *Chem. Soc. Rev.* **2012**, *41*, 1462–1484. [CrossRef]

23. Li, P.-Z.; Wang, X.-J.; Liu, J.; Lim, J.S.; Zou, R.; Zhao, Y.L. A triazole-containing metal-organic framework as a highly effective and substrate size-dependent catalyst for CO$_2$ conversion. *J. Am. Chem. Soc.* **2016**, *138*, 2142–2145. [CrossRef] [PubMed]

24. Ding, M.; Jiang, H.-L. Incorporation of Imidazolium-Based Poly(ionic liquid)s into a Metal-Organic Framework for CO$_2$ Capture and Conversion. *ACS Catal.* **2018**, *8*, 3194–3201. [CrossRef]

25. Zhou, L.-J.; Sun, W.; Yang, N.-N.; Li, P.; Gong, T.; Sun, W.-J.; Sui, Q.; Gao, E.-Q. A Facile and Versatile "Click" Approach Toward Multifunctional Ionic Metal-organic Frameworks for Efficient Conversion of CO$_2$. *ChemSusChem* **2019**, *12*, 2202–2210. [CrossRef] [PubMed]

26. Kuruppathparambil, R.R.; Babu, R.; Jeong, H.M.; Hwang, G.-Y.; Jeong, G.S.; Kim, M.-I.; Kim, D.-W.; Park, D.-W. A Solid Solution Zeolitic Imidazolate Framework as A Room Temperature Efficient Catalyst for the Chemical Fixation of CO$_2$. *Green Chem.* **2016**, *18*, 6349–6356. [CrossRef]

27. Cuesta-Aluja, L.; Masdeu-Bultó, A.M. Iron(III) Versatile Catalysts for Cycloaddition of CO$_2$ to Epoxides and Epoxidation of Alkenes. *ChemistrySelect* **2016**, *1*, 2065–2070. [CrossRef]

28. Yuan, Y.; Li, J.; Sun, X.; Li, G.; Liu, Y.; Verma, G.; Ma, S. Indium-Organic Frameworks Based on Dual Secondary Building Units Featuring Halogen-Decorated Channels for Highly Effective CO$_2$ Fixation. *Chem. Mater.* **2019**, *31*, 1084–1091. [CrossRef]

29. Li, J.; Ren, Y.; Yue, C.; Fan, Y.; Qi, C.; Jiang, H. Highly Stable Chiral Zirconium-Metallosalen Frameworks for CO$_2$ Conversion and Asymmetric C-H Azidation. *ACS Appl. Mater. Interfaces* **2018**, *10*, 36047–36057. [CrossRef]

30. Lu, B.-B.; Yang, J.; Liu, Y.-Y.; Ma, J.-F. A Polyoxovanadate-Resorcin[4]arene-Based Porous Metal-Organic Framework as an Efficient Multifunctional Catalyst for the Cycloaddition of CO$_2$ with Epoxides and the Selective Oxidation of Sulfides. *Inorg. Chem.* **2017**, *56*, 11710–11720. [CrossRef] [PubMed]

31. Cao, J.-P.; Xue, Y.-S.; Li, N.-F.; Gong, J.-J.; Kang, R.-K.; Xu, Y. Lewis Acid Dominant Windmill-Shaped V8 Clusters: A Bifunctional Heterogeneous Catalyst for CO$_2$ Cycloaddition and Oxidation of Sulfides. *J. Am. Chem. Soc.* **2019**, *141*, 19487–19497. [CrossRef]

32. Zhao, Y.-Q.; Liu, Y.-Y.; Ma, J.-F. Polyoxometalate-Based Organic−Inorganic Hybrids as Heterogeneous Catalysts for Cycloaddition of CO$_2$ with Epoxides and Oxidative Desulfurization Reactions. *Cryst. Growth Des.* **2021**, *21*, 1019–1027. [CrossRef]

33. Drake, T.; Ji, P.; Lin, W. Site Isolation in Metal-Organic Frameworks Enables Novel Transition Metal Catalysis. *ACC. Chem. Res.* **2018**, *51*, 2129–2138. [CrossRef]

34. Pei, W.-Y.; Xu, G.; Yang, J.; Wu, H.; Chen, B.; Zhou, W.; Ma, J.-F. Versatile Assembly of Metal-Coordinated Calix[4]resorcinarene Cavitands and Cages through Ancillary Linker Tuning. *J. Am. Chem. Soc.* **2017**, *139*, 7648–7656. [CrossRef]

35. Wei, Y.-S.; Zhang, M.; Zou, R.; Xu, Q. Metal-Organic Framework-Based Catalysts with Single Metal Sites. *Chem. Rev.* **2020**, *120*, 12089–12174. [CrossRef] [PubMed]

36. He, H.; Perman, J.A.; Zhu, G.; Ma, S. Metal-Organic Frameworks for CO$_2$ Chemical Transformations. *Small* **2016**, *12*, 6309–6324. [CrossRef] [PubMed]

37. Singh, G.; Lee, J.; Karakoti, A.; Bahadur, R.; Yi, J.; Zhao, D.; AlBahily, K.; Vinu, A. Emerging trends in porous materials for CO_2 capture and conversion. *Chem. Soc. Rev.* **2020**, *49*, 4360–4404. [CrossRef]

38. Lu, W.; Wei, Z.; Gu, Z.-Y.; Liu, T.-F.; Park, J.; Park, J.; Tian, J.; Zhang, M.; Zhang, Q.; Thomas, G., III; et al. Tuning the structure and function of metal-organic frameworks via linker design. *Chem. Soc. Rev.* **2014**, *43*, 5561–5593. [CrossRef]

39. Jiang, W.; Yang, J.; Liu, Y.-Y.; Song, S.-Y.; Ma, J.-F. A porphyrin-based porous rtl metal-organic framework as an efficient catalyst for the cycloaddition of CO_2 to epoxides. *Chem. Eur. J.* **2016**, *22*, 16991–16997. [CrossRef] [PubMed]

40. Wu, H.; Yang, J.; Su, Z.-M.; Batten, S.R.; Ma, J.-F. An exceptional 54-fold interpenetrated coordination polymer with 103-srs network topology. *J. Am. Chem. Soc.* **2011**, *133*, 11406–11409. [CrossRef]

41. Kalaj, M.; Cohen, S.M. Postsynthetic Modification: An Enabling Technology for the Advancement of Metal-Organic Frameworks. *ACS Cent. Sci.* **2020**, *6*, 1046–1057. [CrossRef] [PubMed]

42. Lu, B.-B.; Chen, X.-Y.; Feng, C.-J.; Chang, J.; Ye, F. Palladium Nanoparticles Immobilized on a Resorcin[4]arene-Based Metal-Organic Framework for Hydrogenation of Nitroarenes. *ACS Appl. Nano Mater.* **2021**, *4*, 2278–2284. [CrossRef]

43. Han, X.; Xu, Y.-X.; Yang, J.; Xu, X.; Li, C.-P.; Ma, J.-F. Metal-Assembled, Resorcin[4]arene-Based Molecular Trimer for Efficient Removal of Toxic Dichromate Pollutants and Knoevenagel Condensation Reaction. *ACS Appl. Mater. Interfaces* **2019**, *11*, 15591–15597. [CrossRef]

44. Liu, J.-H.; Shen, Q.-T.; Yang, J.; Yu, M.-Y.; Ma, J.-F. Polyoxometalate-Templated Cobalt-Resorcin[4]arene Frameworks: Tunable Structure and Lithium-Ion Battery Performance. *Inorg. Chem.* **2021**, *60*, 3729–3740. [CrossRef] [PubMed]

45. Su, K.; Wang, W.; Du, S.; Ji, C.; Zhou, M.; Yuan, D. Reticular Chemistry in the Construction of Porous Organic Cages. *J. Am. Chem. Soc.* **2020**, *142*, 18060–18072. [CrossRef]

46. Lu, B.-B.; Yang, J.; Che, G.-B.; Pei, W.-Y.; Ma, J.-F. Highly Stable Copper(I)-Based Metal-Organic Framework Assembled with Resorcin[4]arene and Polyoxometalate for Efficient Heterogeneous Catalysis of Azide-Alkyne "Click" Reaction. *ACS Appl. Mater. Interfaces* **2018**, *10*, 2628–2636. [CrossRef] [PubMed]

47. Zhang, H.; Yang, J.; Liu, Y.-Y.; Song, S.; Ma, J.-F. A Family of Metal-Organic Frameworks with A New Chair Conformation Resorcin[4]arene-Based Ligand: Selective Luminescent Sensing of Amine and Aldehyde Vapors, and Solvent-Mediated Structural Transformations. *Cryst. Growth Des.* **2016**, *16*, 3244–3255. [CrossRef]

48. Lv, L.-L.; Yang, J.; Zhang, H.-M.; Liu, Y.-Y.; Ma, J.-F. Metal-Ion Exchange, Small-Molecule Sensing, Selective Dye Adsorption, and Reversible Iodine Uptake of Three Coordination Polymers Constructed by A New Resorcin[4]arene-Based Tetracarboxylate. *Inorg. Chem.* **2015**, *54*, 1744–1755. [CrossRef]

49. Lu, B.-B.; Jiang, W.; Yang, J.; Liu, Y.-Y.; Ma, J.-F. Resorcin[4]arene-Based Microporous Metal-Organic Framework as an Efficient Catalyst for CO_2 Cycloaddition with Epoxides and Highly Selective Luminescent Sensing of $Cr_2O_7^{2-}$. *ACS Appl. Mater. Interfaces* **2017**, *9*, 39441–39449. [CrossRef]

50. Sheldrick, G.M. *SHELXS-2014, Program for the Crystal Structure Solution*; University of Göttingen: Göttingen, Germany, 2014.

51. Sheldrick, G.M. *SHELXL-2014, Program for the Crystal Structure Refinement*; University of Göttingen: Göttingen, Germany, 2014.

52. Farrugia, L.J. *WINGX: A Windows Program for Crystal Structure Analysis*; University of Glasgow: Glasgow, UK, 1988.

53. Spek, A.L. PLATON SQUEEZE: A tool for the calculation of the disordered solvent contribution to the calculated structure factors. *Acta Cryst.* **2015**, *C71*, 9–18.

54. Hawxwell, S.M.; Brammer, L. Solvent hydrolysis leads to an unusual Cu(II) metal-organic framework. *CrystEngComm* **2006**, *8*, 473–476. [CrossRef]

55. Murphy, C.A.; Cameron, T.S.; Cooke, M.W.; Aquino, M.A.S. Synthesis and structure of trans-dimethylammonium bis(oxalato)diaquaruthenate(III) tetrahydrate. *Inorg. Chim. Acta* **2000**, *305*, 225–229. [CrossRef]

56. Li, Q.-Q.; Liu, H.; Zheng, T.-T.; Liu, P.; Song, J.-X.; Wang, Y.-Y. The effect of coordinated solvent molecules on metal coordination environments in singlecrystal-to-single-crystal transformations. *CrystEngComm* **2020**, *22*, 6750–6775. [CrossRef]